Food Hydrocolloids 122 (2022) 107078

Contents lists available at ScienceDirect

Food Hydrocolloids

journal homepage: www.elsevier.com/locate/foodhyd

# Competition of rapeseed proteins and oleosomes for the air-water interface and its effect on the foaming properties of protein-oleosome mixtures

Jack Yang [a,b], Claire C. Berton-Carabin [c,d], Constantinos V. Nikiforidis [e], Erik van der Linden [a,b], Leonard M.C. Sagis [b,*]

[a] TiFN, Nieuwe Kanaal 9A, 6709, PA Wageningen, the Netherlands
[b] Laboratory of Physics and Physical Chemistry of Foods, Wageningen University, Bornse Weilanden 9, 6708WG, Wageningen, the Netherlands
[c] Laboratory of Food Process Engineering, Wageningen University, Bornse Weilanden 9, 6708WG, Wageningen, the Netherlands
[d] INRAE, UR BIA, F-44316, Nantes, France
[e] Laboratory of Biobased Chemistry and Technology, Wageningen University, Bornse Weilanden 9, 6708WG, Wageningen, the Netherlands

ARTICLE INFO

*Keywords:*
Rapeseed proteins
Oleosomes
Oil bodies
Surface rheology
Foams
Atomic force microscopy

ABSTRACT

There is an increasing interest to apply oleosomes (plant oil storage organelles) as natural oil droplets in food systems. Lipids are usually known to be detrimental for protein-stabilised foams due to the weakening of interactions between adsorbed proteins, or by forming oil bridges between two protein surfaces. Both mechanisms can lead to film rupture, and thereby destabilise protein-stabilised foams. Little is known about the influence of oleosomes on protein-stabilised interfaces and foams. Therefore, these properties were studied for rapeseed protein–oleosome mixtures at various protein concentrations and ratios. At 0.1 and 0.2% (w/w) protein content, oleosomes were found to co-adsorb with proteins at the interface, followed by rupture of oleosomes and release of triacylglycerols and phospholipids. This led to weaker in-plane interactions between adsorbed proteins. As a result, the foamability and foam stability of protein-oleosome systems were substantially lower compared to systems made with pure proteins. At 0.5 and 1.0% (w/w) protein content, the rapeseed proteins were found to dominate the interfacial properties. The proteins formed a dense solid-like layer at such high concentrations, which prevented the oleosomes from co-adsorbing at the interface. Also, in foam systems at high protein concentrations, the proteins seemed to outcompete the oleosomes for the interface, leading to higher foam stability. Here, we have demonstrated that the detrimental influence of oleosomes on protein-stabilised interfaces and foams can be controlled by varying the amount of oleosomes and rapeseed proteins in the mixture, which is a promising outcome to further utilise oleosomes in aerated food systems.

## Credit author statement

Jack Yang: Conceptualisation, Methodology, Investigation, Validation, Visualisation, Writing – Original Draft; Claire C. Berton-Carabin: Conceptualisation, Methodology, Writing – Review & Editing; Costantinos V. Nikiforidis: Conceptualisation, Methodology, Writing – Review & Editing; Erik van der Linden: Writing – Reviewing & Editing, Funding acquisition; Leonard M. C. Sagis: Conceptualisation, Methodology, Supervision, Writing – Review & Editing.

## 1. Introduction

Oilseeds are widely cultivated for oil production and are essential in a healthy human diet (Damude & Kinney, 2008; Lin et al., 2013). Examples of such plant crops are soybeans, sunflower seeds and rapeseeds. Their oil is generally extracted by pressing, followed by an organic solvent-based extraction step (Danlami, Arsad, Zaini, & ; Tasan, Gecgel, & Demirci, 2011). Such processing disrupts the naturally occurring oil reservoirs in plants, known as oleosomes, oil bodies, or lipid droplets (Abdullah, Weiss, & Zhang, 2020; Karefyllakis, Van Der Goot, & Nikiforidis, 2019; Nikiforidis, 2019). Oleosomes are natural oil droplets (diameter 0.2–10.0 μm) of triacylglycerols (TAGs), which are surrounded by a protective monolayer of phospholipids with anchored membrane proteins, mostly oleosins (Fig. 1) (Frandsen, Mundy, & Tzen, 2001; Nikiforidis, 2019; Tzen, 2012; Tzen, Cao, Laurent, Ratnayake, & Huang, 1993). Oleosomes can be extracted without physical disruption

* Corresponding author.
*E-mail addresses:* jack.yang@wur.nl (J. Yang), leonard.sagis@wur.nl (L.M.C. Sagis).

https://doi.org/10.1016/j.foodhyd.2021.107078
Received 30 April 2021; Received in revised form 26 July 2021; Accepted 30 July 2021
Available online 3 August 2021

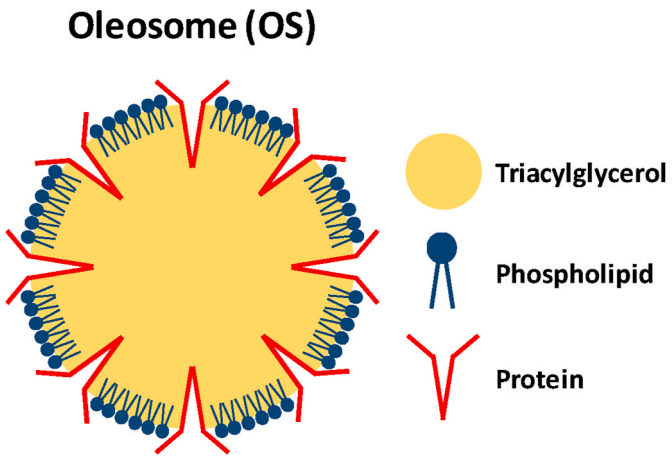


**Fig. 1.** Schematic overview of the oleosome structure. The components in the illustration are not to scale.

by aqueous mild purification methods (Romero-guzman, Louis, Kyriakopoulou, Boom, & Nikiforidis, 2020), and possess exceptional high chemical and physical stability against lipid oxidation and droplet coalescence (Ding, Wen, et al., 2020; Ding, Xu, et al., 2020; Kapchie, Yao, Hauck, Wang, & Murphy, 2013; Karkani, Nenadis, Nikiforidis, & Kiosseoglou, 2013).

The food industry, instead of exploiting the exceptional properties of oleosomes, and use them as such in emulsion systems; the current food emulsion production processes focus on the creation of "artificial" oil droplets by emulsifying the oleosome extracted oil with emulsifiers. If the use of intact oleosomes for food applications could be facilitated, the processing steps of oil extraction and oil droplet formation can be avoided. Therefore, oleosomes can play an important role in the sustainable food transition, in applications such as natural emulsions in liquid/solid foods, or even as a functional component in oil structuring (Ishii et al., 2017; Iwanaga et al., 2007; Nikiforidis, 2019).

The aforementioned food applications are obvious for oleosomes, but oils/lipids could also be applied as a functional ingredient in other systems, such as foams, which is the focus of this work. Foams are air bubbles entrapped in continuous liquid or solid matrices, such as milk foams and ice cream (Damodaran, 2005). In food foam systems, the air-water interface is often stabilised by proteins that form stiff and viscoelastic solid-like interfacial layers (Narsimhan & Xiang, 2018; Yang, Faber, et al., 2020), which is an important attribute in forming stable foams (Dickinson, 1999; Foegeding, Luck, & Davis, 2006; Yang, Lamochi Roozalipour et al., 2021). Polar lipids, such as phospholipids, can compete with proteins for the interface, forming mixed interfaces, or even displace the proteins from the interface (Dickinson, 2011; Waninge et al., 2005; Zhang, Cui, & Li, 2002). As a result, the proteins are impaired in the formation of strong interfacial layers, which may lead to poor foaming properties (Wilde et al., 2003). Also, the TAGs in the oleosome core can act as anti-foaming agents in the thin films by bridging two air bubbles, thereby inducing coalescence of the air bubbles (Denkov, 2004; Denkov & Marinova, 2006).

However, the interfacial behaviour of oleosomes is different from that of free lipids, as both phospholipids and TAGs are enclosed in the colloidal structure of the oleosomes. For soybean oleosomes, a slow initial adsorption phase was demonstrated in a Langmuir trough, due to the relatively slow diffusion towards the air-water interface. After approaching the air-water interface, oleosomes were able to adsorb at the interface, followed by rupture of the phospholipid/protein membrane (Waschatko, Junghans, & Vilgis, 2012; Waschatko, Schiedt, Vilgis, & Junghans, 2012). The different components started to phase separate into TAG-rich and membrane-rich regions, which we also demonstrated in our previous work by studying the topography of the Langmuir-Blodgett films (Yang, Waardenburg, et al., 2021). In our previous work, oleosome-stabilised air-interfaces were weaker and more mobile compared to protein-stabilised interfaces, due to weak in-plane interactions. Desorption and adsorption of interfacial material were observed upon compression and expansion of the interfacial area. Mixing of whey proteins and oleosomes formed a mixed interface, where whey proteins surrounded the TAG-rich regions. When oleosomes were present, they dominated the rheological response of the mixed interfaces.

The influence of oleosomes on the protein interfacial layer was not observed in the foaming properties of mildly-purified rapeseed protein extracts, which contained about 8% (w/w) oleosomes (Yang, Faber, et al., 2020). A defatted rapeseed protein extract had similar foaming properties as a non-defatted protein extract, thus indicating that oleosomes at this concentration did not hamper protein foaming properties. However, the previous studies were limited to one protein-to-oleosome ratio and were performed at relatively low bulk concentrations (<0.2% w/w) compared to real food systems. At different absolute amounts of proteins and different protein-oleosome ratios, it is not yet clear which component would dominate the functional properties of the total mixture.

Therefore, we aim to investigate rapeseed protein and oleosome mixtures for their interfacial and foaming properties at various bulk concentrations and protein-to-oleosome ratios. Oleosomes and proteins were extracted from rapeseeds, and systematically mixed. The rapeseed protein-oleosome mixtures were studied by surface dilatational rheology, and microstructure imaging by performing atomic force microscopy on Langmuir-Blodgett films. Finally, the mixtures were characterised for their foaming properties. A comprehensive study on the effect of oleosomes on protein-stabilised foams provides new insights on the necessity of purifying proteins from oleosomes, and further expands the possibilities for using oleosomes as a sustainable ingredient in foods.

## 2. Experimental section

### 2.1. Materials

Untreated Alizze rapeseeds were purchased from a local seed producer. All chemicals (Sigma-Aldrich, USA) were used as received. Ultrapure water (MilliQ Purelab Ultra, Germany) was used in all experiments.

### 2.2. Sample preparation

#### 2.2.1. Rapeseed protein extraction

Rapeseed protein concentrate (**RPC**) was prepared with the method of Ntone et al. (Ntone, Bitter, & Nikiforidis, 2020). Dehulled rapeseed kernels were soaked for 4 h at pH 9.0 in a rapeseed-to-water ratio of 1:8 (w:w). Afterwards, the mixture was blended for 2 min at max speed in a kitchen blender (Waring Commercial, 400 W, USA) to obtain a rapeseed slurry, and the solids were removed using a twin-screw press. The pH of the liquid extract was re-adjusted to 9.0 after the completion of each previously mentioned step. The supernatant was centrifuged for 30 min at 10,000×*g* (4 °C), which resulted in a three-layer system: a cream layer on top, a pellet with solids, and a middle layer containing the soluble proteins and other solutes. The middle layer was recovered and diafiltrated over a 5-kDa membrane to remove minerals, sugars and free phenols. The diafiltrated sample was freeze-dried, which yielded a mildly purified RPC. The protein extract was further purified to obtain the soluble fraction at the studied conditions by dispersing 10% (w/w) mildly purified RPC in 20 mM sodium phosphate buffer (pH 7.0). The dispersion was adjusted to pH 7.0 and stirred overnight at 4 °C. Afterwards, the dispersion was centrifuged twice for 30 min at 16,000×*g* (20 °C) and filtered over a 0.22 μm syringe filter. The supernatant was freeze-dried for further analysis and labelled as rapeseed protein concentrate (RPC).

*2.2.2. Oleosomes extraction*

A rapeseed slurry was produced, as mentioned in the previous paragraph. The pH of the slurry was adjusted to 9.0, and the slurry was passed through a cheesecloth to remove the solids. The pH was adjusted once more to 9.0, and the sample was centrifuged for 30 min at 10,000×*g* (4 °C). The cream layer was resuspended in ultrapure water at a 1:5 (w/v) ratio, stirred for 15 min, and centrifuged for 30 min at 10,000×*g* (4 °C). A second re-dispersion step was performed with 20 mM sodium phosphate buffer (pH 7.0), followed by another centrifugation step. The final cream layer containing oleosomes was recovered and diluted with buffer based on dry matter content. Large aggregated clusters of oleosomes were broken up by a high-speed mixing step of 30 s at 5000 rpm with a T25 Ultra-turrax (IKA, Germany). A preservative (sodium azide) was added to the oleosome extract (**OS**), and the sample was used in experiments for a maximum of 5 days while stored at 4 °C.

*2.2.3. Compositional analysis*

The protein content was measured in a Flash EA 1112 Series Dumas (Interscience, The Netherlands). The nitrogen content of the samples was obtained, which was converted into protein content using a conversion factor of 5.7 (Fetzer, Herfellner, & Eisner, 2019). These measurements were performed in triplicate. The oil content was determined by drying the samples overnight at 60 °C, followed by solvent (petroleum ether) extraction for 6 h in a Soxhlet. The oil content was calculated by weighing the initial sample and the oil in the collection flasks. The measurements were performed in duplicate.

*2.2.4. Dissolving samples*

RPC was dissolved in 20 mM sodium phosphate buffer (pH 7.0) at protein concentrations ranging from 0.1 to 2% (w/w), and the sample was stirred for 4 h at room temperature. The OS were diluted in the same buffer to concentrations ranging from 0.002 to 2% (w/w). RPC-OS mixtures were prepared by mixing pure RPC and OS in a 1:1 (v:v) ratio. The mixtures had rapeseed protein concentrations of 0.1, 0.2, 0.5, and 1.0% (w/w), and protein-to-OS (w/w) ratios of 100:1, 10:1, and 1:1.

*2.2.5. Determination of adsorption behaviour and surface dilatational properties*

The air-water interfacial properties were investigated using drop tensiometers. A profile analysis tensiometer PAT-1M (Sinterface Technologies, Germany) was used to perform time and frequency sweeps. A hanging droplet with an area of 20 $mm^2$ was created at the tip of a needle, and the shape of the droplet was analysed and fitted with the Young-Laplace equation to calculate the surface tension. The droplet was always equilibrated for 3 h before performing any deformation of the droplet area. Frequency sweeps were performed by increasing the oscillatory deformation frequency from 0.002 – 0.1 Hz with a fixed amplitude of 3%. An automated drop tensiometer (ADT, Teclis, France) was used to perform amplitude sweeps, and the ADT was operated similarly to the PAT-1M. A major difference was the droplet size, which had an area of 15 $mm^2$ in the ADT. The droplet was again subjected to 3 h of waiting time before performing the amplitude sweep, where the amplitude was increased from 2 to 50% at a fixed frequency of 0.02 Hz. All measurements were performed at least in triplicates at 20 °C. The amplitude sweep was further analysed by plotting Lissajous plots of the surface pressure ($\Pi = \gamma\text{-}\gamma_0$) over the deformation ($(A\text{-}A_0)/A_0$). Here, $\gamma$ and $A$ are the surface tension and area of the deformed interface, $\gamma_0$ and $A_0$ are the surface tension and area of the non-deformed interface. Lissajous plots were made from the middle three oscillations of each amplitude cycle.

*2.2.6. Preparation of Langmuir-Blodgett films*

*2.2.6.1. Langmuir-Blodgett films of RPC-OS mixtures.* A Langmuir trough (KSV NIMA/Biolin Scientific Oy, Finland) was used to produce Langmuir-Blodgett (**LB**) films of interfacial films stabilised by RPC and RPC-OS mixtures. Samples with RPC contained 0.1% (w/w) protein, and the protein-oleosome mixtures had RPC concentrations varying from 0.05 to 0.1% (w/w) and OS concentrations varying from 0.001 to 0.05% (w/w). The Langmuir trough was filled with 20 mM phosphate buffer (pH 7.0), and 200 μL of sample solution was injected at the bottom of the trough with a gas-tight syringe. A 3 h waiting step was necessary to allow adsorption of the surface-active material at the interface. The surface pressure was measured with a Wilhelmy plate (platinum, perimeter 20 mm, height 10 mm). Afterwards, the interfacial film was compressed with Teflon barriers moving at 5 mm/min to a target surface pressure of 21 mN/m. The surface pressure was kept constant, while the interfacial layer was deposited on a freshly cleaved mica sheet (Highest Grade V1 Mica, Ted Pella, USA) at a withdrawal speed of 1 mm/min. All films were produced in duplicate and dried in a desiccator.

*2.2.6.2. Langmuir-Blodgett films to study potential displacement of RPC-proteins by OS.* The Langmuir trough was similarly prepared and operated as described in the previous paragraph. A major difference is the separate introduction of RPC and OS. First, 200 μL of 0.01–0.1% (protein w/w) RPC solutions were spread on top at the surface using a gas-tight syringe. The interfacial layer was equilibrated for 30 min, and afterwards, the layer was compressed until a target surface pressure of 5, 10, 15, 20, or 25 mN/m. The target surface pressure was maintained by constantly compressing the interface until the surface pressure was constant without further compression. Afterwards, 100 μL of OS extract was injected at the bottom of the trough, i.e., below the RPC-stabilised film. The concentration was determined by the surface area of the Langmuir film, which was varied for each replicate, as 0.001% of OS/100 μL was injected per $cm^2$ of surface area. Oleosomes were found to diffuse and adsorb at the interface after roughly 1 h. Therefore, an adsorption time of 1.5 h was applied after infusion of the OS in the subphase. Finally, Langmuir-Blodgett films were produced, as described in the previous section. All films were prepared in duplicate and dried in a desiccator before analysis.

*2.2.7. Determination of interfacial microstructure by AFM*

The topography of the LB films was analysed with atomic force microscopy (**AFM**, MultiMode 8-HR, Bruker, USA) in tapping mode using a Scanasyst-air model non-conductive pyramidal silicon nitride probe (Bruker, USA) with a normal spring constant of 0.40 N/m and a lateral scan frequency of 0.977 Hz. The films were scanned over an area of 2 × 2 $\mu m^2$ with a lateral resolution of 512 x 512 $pixels^2$. At least two locations were scanned on the films to ensure good representativeness.

*2.2.8. Determination of foaming properties*

The foaming ability of the samples was analysed by whipping using an aerolatte froth (Aerolatte, UK) connected to an overhead stirrer. Aliquots of 15 mL solution were whipped for 2 min at 2,000 rpm in plastic tubes (ø = 3.4 cm), and the top and the bottom of the foam were directly marked on the tube. The difference was measured using a ruler, and a foam volume was calculated with the tube diameter. From the foam volume, the overrun (%) was calculated by dividing the foam volume (mL) by the liquid volume (15 mL) times 100. The foam stability of the samples was analysed in a Foam scan (Teclis, France). Foams with a volume of 400 mL were produced from 40 mL of sample in a glass cylinder (ø = 6 cm) by sparing nitrogen gas through a metal frit (27 μm pore size, 100 μm distance between centres of pores, square lattice) at a gas flow rate of 400 mL/min. A camera monitored the foam volume until half of the foam volume decayed, and this time point is also known as the foam volume half-life time. The machine was equipped with an SLR lens to record detailed images of air bubbles, which were analysed using DIPlip and DIPimage image analysis software (TU Delft, the Netherlands) to quantify the average air bubble size. All experiments were performed at least in triplicate at room temperature.

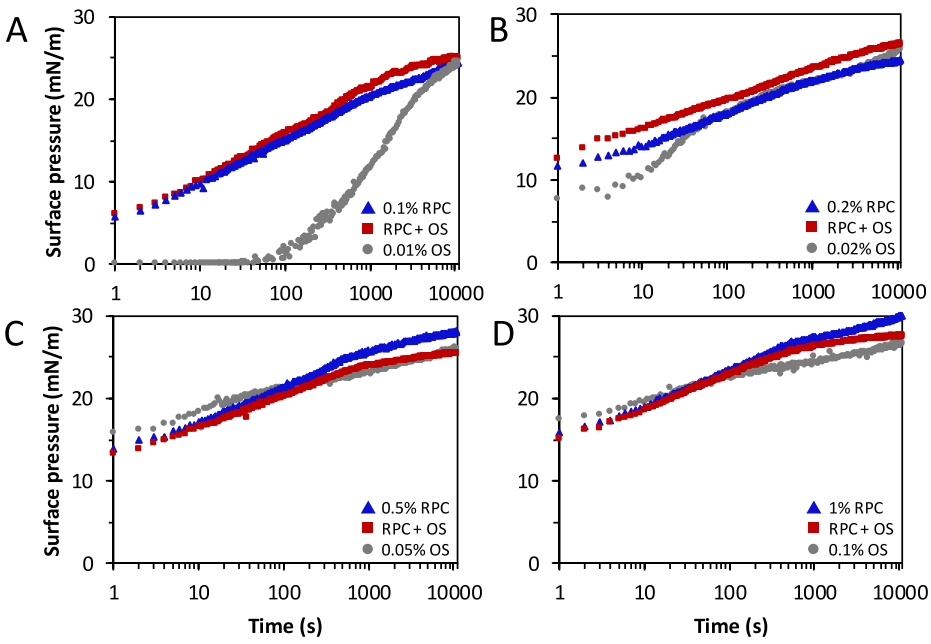


**Fig. 2.** Surface pressure as a function of time of interfacial films stabilised by RPC (blue triangles), OS (grey circles), and RPC-OS mixtures (red squares) in buffer (20 mM $PO_4$, pH 7.0). The concentrations of RPC and OS are shown in the legend of each graph, and these concentrations are also applied in the RPC-OS mixtures. The surface pressure isotherms represent an average of at least three replicates. The standard deviation was below 5%. (For interpretation of the references to colour in this figure legend, the reader is referred to the Web version of this article.)

## 3. Results and discussion

### 3.1. Protein and oleosome extraction

Rapeseed proteins, napin and cruciferin, were extracted with a mild-purification method to obtain a rapeseed protein concentrate (**RPC**) that retained the native protein structure and had a protein content of 77.8 ± 1.9% (w/w) (Ntone et al., 2020; Yang, Faber, et al., 2020). The protein purity increased by roughly 6% compared to a previously produced RPC in our earlier work (Yang, Faber, et al., 2020) due to an additional filtration step in the current work. The filtration step (partly) removed oleosome (**OS**) flocculates between 2 and 300 μm. As a result, the oil content of the RPC was a minor 0.8 ± 0.3% (w/w). The obtained OS extract contained 88.5 ± 3.8% (w/w) oil and 7.2 ± 0.3% (w/w) protein and had a droplet size distribution between 0.2 – 20.0 μm with a $d_{3,2}$ of 0.8 μm (Yang, Waardenburg, et al., 2021).

### 3.2. Interfacial properties of rapeseed protein – oleosome mixtures

#### 3.2.1. Adsorption behaviour

The adsorption behaviour of RPC, OS, and RPC-OS mixtures at an air-water interface was studied (Fig. 2), and the protein bulk concentration of RPC was varied between 0.1 – 1.0% (w/w), while OS was added to obtain a 10:1 RPC-to-OS ratio. This ratio was chosen, as a comparable ratio was found in the mildly-derived RPC in our previous work (Yang, Faber, et al., 2020). Pure RPC at all concentrations led to an immediate increase of surface pressure with values between 5 – 15 mN/m at 1 s, followed by a continuous increase to values up to 30 mN/m after 3 h of adsorption. We should keep in mind that the RPC contains roughly 20% non-proteinaceous material. We do not expect high amounts of surface active components in this fraction, as small molecular surfactants should be removed in the extensive diafiltration step. The OS had a different behaviour at lower concentrations, such as 0.01% (w/w) OS (Fig. 2A). For this sample, a lag time was observed in the first 50 s, showing that the amount of stabiliser on the interface is insufficient to increase the surface pressure. Afterwards, the surface pressure increased rapidly to similar values as with the 0.1% (w/w) RPC after 3 h.

The adsorption behaviour of OS is different from that of rapeseed proteins, as OS are larger structures, and thus have a lower diffusion rate towards the interface. The OS can rupture after adsorption, followed by spreading of the membrane (made of phospholipids and proteins) and triacylglycerol (**TAG**) core over the interface (Waschatko, Schiedt, et al., 2012). These phenomena are shown in the adsorption isotherm of 0.02% (w/w) OS, where a slow adsorption phase in the first 10 s was followed by a rapid increase up to 70 s due to OS adsorption. After 70 s, the slope decreased due to OS rupture and rearrangements of the components at the interface. At higher concentrations of 0.05 and 0.10% (w/w) OS (Fig. 2C and D), OS adsorbed at a higher rate, comparable to that observed with pure RPC. The findings at higher OS concentrations should be interpreted with caution, as impurities in the OS extract, such as storage proteins and phenols, could significantly contribute to the adsorption behaviour.

Mixing RPC and OS showed two types of behaviour, and the first type is present in Fig. 2A and B. In Fig. 2A, the RPC-OS (0.10% RPC – 0.01% w/w OS) adsorption kinetics coincided with that of the pure RPC up to 50 s, indicating adsorption of mainly rapeseed proteins, which is expected, as pure OS showed a lag phase in this period. After 50 s, the slope measured for the RPC-OS mixture was higher than pure RPC, suggesting a contribution of OS, as the pure OS curve also showed an increase of surface pressure from this time point. Such co-adsorption is also found for a higher concentration (0.20% RPC – 0.02% w/w OS), as the mixture led to a higher surface pressure than with pure RPC or OS. The surface pressure kinetics at higher concentrations (0.5% RPC – 0.05% OS & 1% RPC – 0.1% w/w OS) showed a distinctly different behaviour, as the curve of the mixtures first followed the pure RPC curve in the initial ±300 s. Afterwards, the slope of the mixtures was lower compared to pure RPC. At such high concentrations, the RPC and OS seemed to start competing for the interfacial area, perhaps leading to a partial displacement of RPC. An alternative explanation could be that the components segregate after adsorption (2D phase-separation) at these higher concentrations, leading to a heterogeneous interfacial microstructure. Additionally, proteins and oleosomes are not expected to interact in the bulk, as both rapeseed proteins and oleosomes are negatively charged at pH 7.0 (Romero-Guzmán, Köllmann, Zhang, Boom, & Nikiforidis, 2020; Yang, Faber, et al., 2020). The structure and mechanical properties of the interfacial film were further assessed by performing rheological experiments.

#### 3.2.2. Surface dilatational rheology

The surface dilatational moduli of interfacial films stabilised by RPC

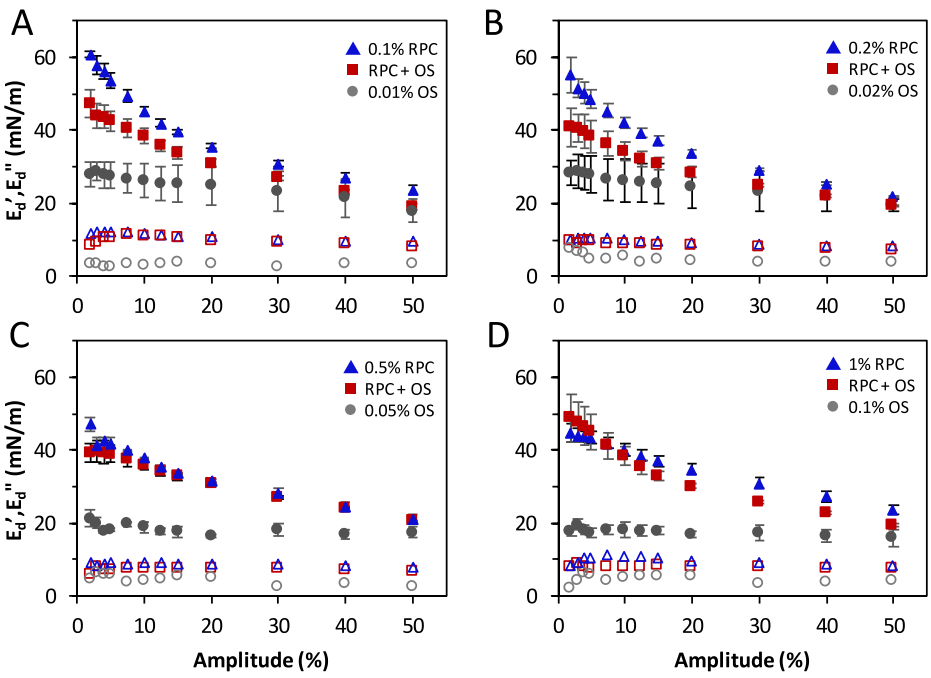


**Fig. 3.** The surface dilatational storage ($E_d$') and loss ($E_d$") moduli as a function of the deformation amplitude for interfacial films stabilised by RPC (blue triangles), OS (grey circles), and RPC-OS mixtures (red squares) in buffer (20 mM $PO_4$, pH 7.0). The concentrations of RPC and OS are shown in the legend of each graph, and these concentrations are also present in the RPC-OS mixtures. The closed symbols depict the storage modulus ($E_d$'), and open symbols depict the loss modulus ($E_d$"). The averages and standard deviations are the result of at least three replicates. (For interpretation of the references to colour in this figure legend, the reader is referred to the Web version of this article.)

and RPC-OS mixtures were obtained from an amplitude sweep using drop tensiometry (Fig. 3). At all RPC concentrations (0.1–1% w/w), rapeseed protein-stabilised interfacial films showed a decline of storage modulus (***$E_d$'***) from 42 – 60 mN/m (2% deformation) to 22–24 mN/m (30% deformation) with increasing amplitude, indicating the presence of a nonlinear viscoelastic (**NLVE**) regime. Amplitude-dependent moduli suggest an increased disruption of the interfacial structure at higher deformations. The amplitude-dependence of $E_d$' in combination with a substantially lower loss modulus (***$E_d$"***) indicates the formation of a viscoelastic solid-like layer. Formation of such interfaces was previously demonstrated for rapeseed proteins at both air-water and oil-water interfaces (Ntone et al., 2020; Yang, Faber, et al., 2020). In this previous work, we also observed a decrease of surface moduli upon increasing protein bulk concentration, which we attributed to the presence of non-proteinaceous components, such as phenols and oleosomes. A similar trend was also found in this work, where the $E_d$' decreased with higher RPC concentrations. Interfacial films stabilised by OS had a distinctly different rheological behaviour, as the $E_d$' were low and nearly independent of the applied deformation. OS-stabilised interfaces were more mobile with an increased mass exchange between bulk and interface upon deformation (Yang, Waardenburg, et al., 2021). This behaviour was associated with the low in-plane interactions between the interfacial stabiliser at an OS-stabilised interface.

The mixtures led to different behaviour, depending on the total protein content. At a fixed protein content of 0.1 and 0.2% (w/w) (Fig. 3A and B), the RPC–OS–stabilised interfaces had lower $E_d$' than pure RPC-stabilised ones. The moduli decreased due to the presence of OS in the bulk, and most likely at the air-water interface. A different influence of the OS was observed at higher concentrations (0.5 and 1% w/w) (Fig. 3C and D), as the moduli of interfaces stabilised by RPC-OS mixtures coincided remarkably with those of pure RPC-stabilised interfaces. This implies a less detrimental effect of OS on the rheological

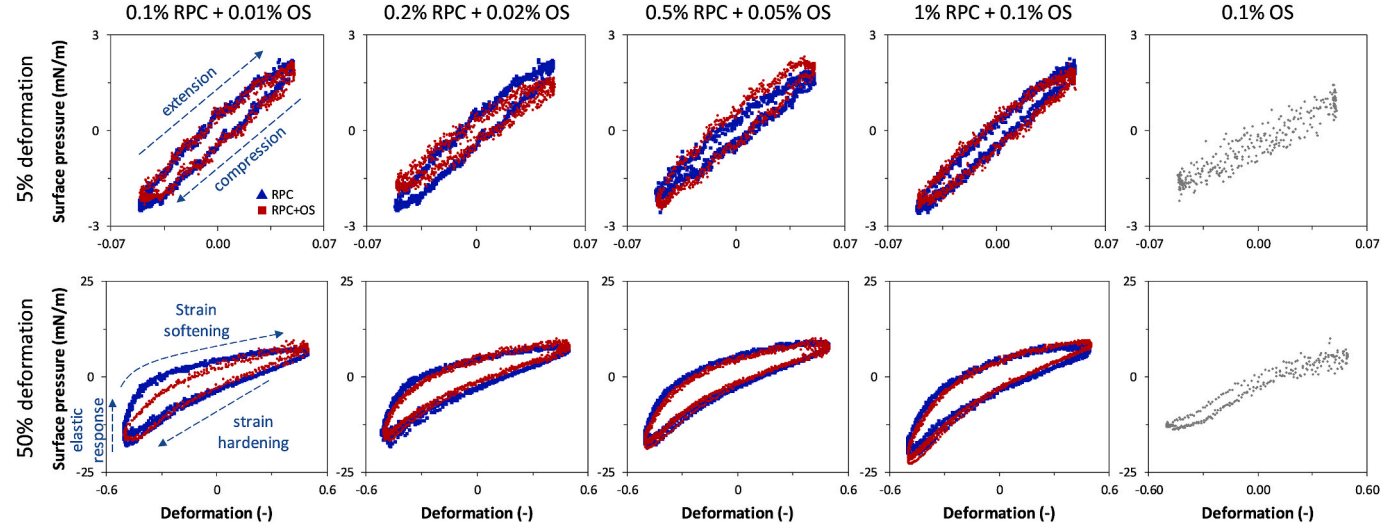


**Fig. 4.** Lissajous plots of surface pressure as a function of the applied deformation, obtained from amplitude sweeps of air-water interfacial films stabilised by RPC (blue triangles), OS (grey circles), and RPC-OS mixtures (red squares). For clarity, one representative plot is shown for each sample, but comparable plots were obtained on at least three replicates. (For interpretation of the references to colour in this figure legend, the reader is referred to the Web version of this article.)

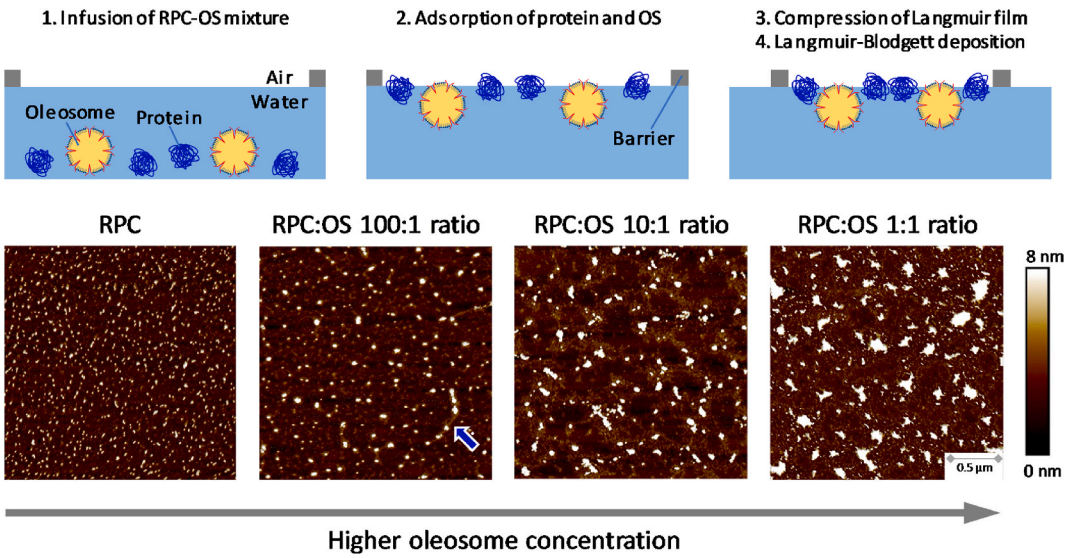


**Fig. 5.** A schematic overview of the production of Langmuir-Blodgett films, and the AFM images of LB-films made from RPC and RPC-OS mixtures. The films were produced at a target surface pressure of 21 mN/m. The images are representative of at least four scans on two independently produced films.

properties of the RPC-stabilised interface at higher protein concentrations, at a constant RPC-to-OS ratio. The interactions between the interfacial stabilisers were further examined by constructing Lissajous plots.

### 3.2.3. *Lissajous plots*

The dilatational surface moduli obtained from amplitude sweeps are calculated from the intensity and phase shift of the first harmonic of the Fourier transform of the surface stress signal. Only incorporating the first harmonic results in neglecting the contributions of higher-order harmonics present in the surface stress signal in the NLVE regime, caused by disruptions of the interfacial microstructure at large deformations. The contribution of higher harmonics was previously analysed by constructing Lissajous plots, where the surface stress is plotted against applied deformation (Ewoldt, Hosoi, & McKinley, 2007). Previously, Lissajous plots were demonstrated as a useful tool to analyse the contribution of higher-order harmonics that are generated at large deformations (Humblet-Hua, van der Linden, & Sagis, 2013; Yang, Faber, et al., 2020; Yang, Thielen, Berton-Carabin, van der Linden, & Sagis, 2020).

The results of the amplitude sweep were transformed into Lissajous plots and are depicted in Fig. 4. All Lissajous plots at 5% deformation amplitude showed narrow and symmetric ellipses, suggesting an interfacial layer where the elastic component dominated the stress response. By increasing the deformation amplitude to 50%, the Lissajous plots became asymmetric due to disruption of the interfacial microstructure. At such large deformations, higher-order harmonics are generated that are well illustrated by the shape of Lissajous plots. Several rheological phenomena are present in the plots and are highlighted in the 50% deformation plot of a 0.1% RPC-stabilised interface. At the start of the extension cycle (at −0.50 deformation, bottom-left corner), we observed a steep increase in surface pressure (nearly vertical) due to a predominantly elastic response. Afterwards, the steep increase was followed by a phase with a decreasing slope, showing a gradual (intra-cycle) strain softening of the interfacial microstructure upon further extension of the interfacial area. Here, the elastic component started to diminish, and the viscous component started dominating the response, implying that the interfacial microstructure started flowing.

A distinct behaviour can be examined in compression of the interface, as the surface pressure increased steeply to a higher maximum surface pressure (−18 mN/m) compared to the value in extension (+6 mN/m), which is known as intra-cycle strain hardening. Strain hardening was previously attributed to the concentration of adsorbed proteins upon compression. As a result, dense protein clusters would form and start jamming (Yang, Thielen, et al., 2020). The depicted rheological behaviour suggests the formation of a viscoelastic solid-like layer by RPC, probably due to strong in-plane interactions between rapeseed proteins at the air-water interface. Interestingly, the initial elastic response became less evident at higher protein concentrations (at 50% deformation), and the plots also became slightly narrower. This would imply slightly weakened in-plane interactions between proteins at these higher protein concentrations (≥0.5% w/w).

The OS-stabilised interface showed a substantially narrower Lissajous plot at 50% deformation compared to RPC. The plot also revealed a slight strain softening in compression that we previously related to the pushing out of interface stabiliser into the bulk, due to weak in-plane interactions between molecules at the OS-stabilised interface. In previous work, rupture of OS was demonstrated at the air-water interface, leading to a heterogeneous interface with TAG-rich regions and membrane fragments. Especially phospholipids and TAGs largely hamper interactions between other stabilisers at the interface, thus weakening the interfacial layer, which was demonstrated for protein interfaces (Caro, Niño, & Patino, 2009; Denkov & Marinova, 2006; Maldonado--Valderrama & Patino, 2010; Wilde et al., 2003).

The Lissajous plot showing 50% deformation of an interfacial film stabilised by a 0.1% (w/w) RPC – 0.01% (w/w) OS mixture was considerably narrower compared to the plot for pure RPC at 0.1% (w/w), implying the formation of a weaker layer due to impaired in-plane interactions among adsorbed proteins. Such changes of rheological behaviour in the presence of OS imply the interference of phospholipids and TAG of OS (after rupture) on the layer formation of rapeseed proteins, which by itself formed stiff and viscoelastic solid-like layers. Similar behaviour was observed in whey protein-OS mixtures, as the OS weakened the interactions between whey proteins by forming large phospholipid/TAG-rich regions at the interface, leading to 2D phase separation of proteins and lipids at the interface (Yang, Waardenburg, et al., 2021). Also, pure phospholipids and surfactants are known to form concentrated and laterally segregated regions at the interface, thereby reducing the protein interactions at the interface (Glomm, Volden, Halskau, & Ese, 2009; Mackie, Gunning, Wilde, & Morris, 1999; Zhang et al., 2002).

At higher protein concentrations, OS had a limited effect on the rheological properties of the RPC–OS–stabilised interface. From 0.5% (w/w) RPC onwards, the OS-protein mixtures led to nearly overlapping

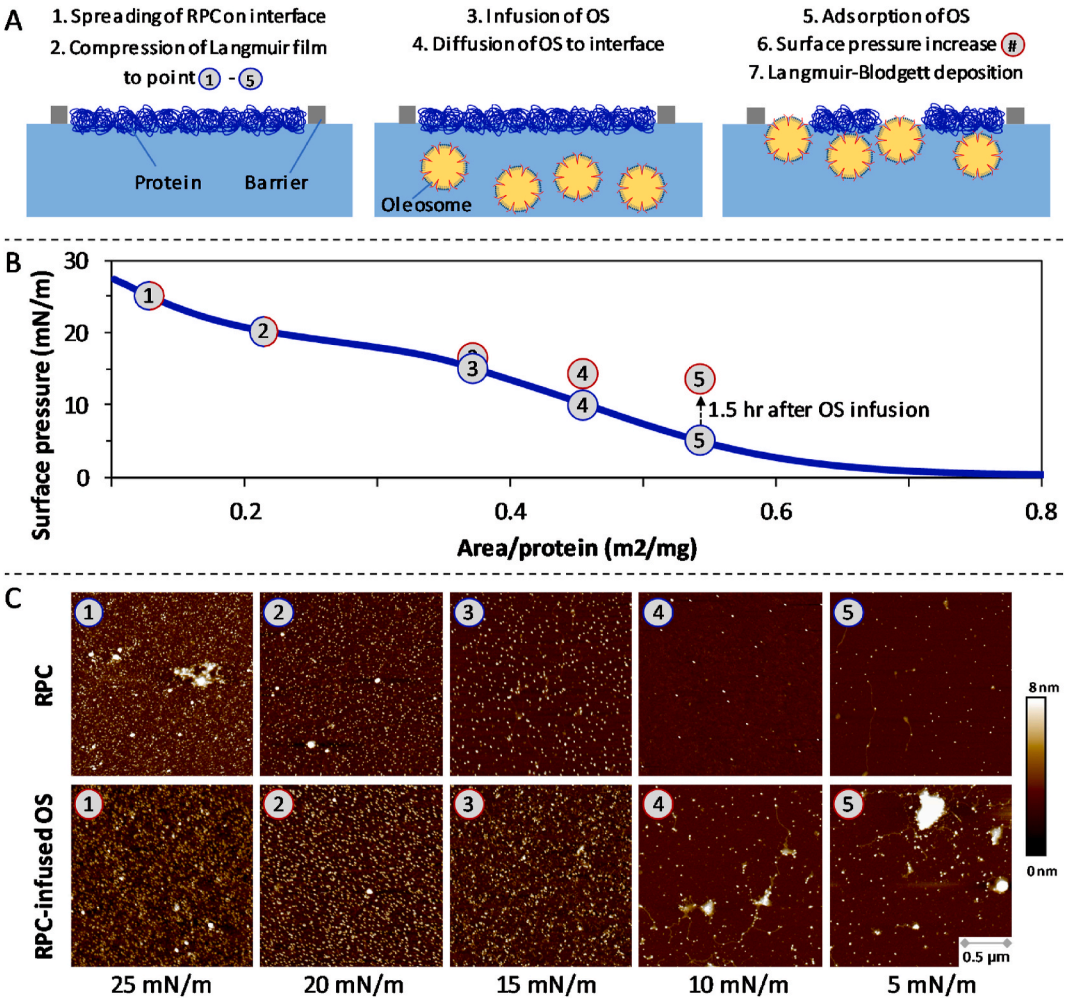


**Fig. 6.** (A) A schematic overview of the production of the Langmuir-Blodgett films. (B) Surface pressure isotherm obtained from a Langmuir trough of an RPC-stabilised film. RPC interfaces were produced at one of the five marked points (blue circles), and OS was injected at the bottom to study potential adsorption/displacement. After allowing the OS to diffuse towards the interface, the surface pressure increases, shown by the red circles. The Langmuir films were deposited on a substrate to create Langmuir-Blodgett films. (C) AFM scans of these films are shown, and the numbers correspond to the moment of film samples in the surface pressure isotherm. Pure RPC films were also included. The isotherm is an average of two replicates, and the error was below 5%. The images are representative of at least four scans on two independently produced films. (For interpretation of the references to colour in this figure legend, the reader is referred to the Web version of this article.)

Lissajous plots compared to pure RPC. The detrimental effect of OS on a protein-stabilised interface is concentration-dependent (at a fixed RPC-to-OS ratio), and might be related to the findings in the adsorption behaviour (Fig. 2). At lower protein concentrations of 0.1 and 0.2% (w/w), we demonstrated co-adsorption of both rapeseed proteins and OS, whereas the adsorption of rapeseed proteins seemed to be more predominant at higher protein concentrations of 0.5 and 1.0% (w/w). A mixed interface after co-adsorption (0.1 and 0.2% RPC) could increase the weakening effect of OS on the rapeseed proteins' connectivity in the interfacial layer, whereas an interface with more RPC (0.5 and 1.0% RPC), thus less OS, would result in less decrease in moduli. To summarise, OS can negatively influence the in-plane interactions of adsorbed rapeseed proteins, leading to weaker interfacial layers. This behaviour is concentration-dependent, as RPC is more dominant at higher concentrations (>0.2% w/w).

### 3.2.4. *Interfacial microstructure*

Imaging the interfacial microstructure can contribute to a better understanding of the rheological properties of RPC-OS mixture-stabilised interfacial layers. Interfacial films were produced in a Langmuir trough by injecting RPC-OS mixtures with various ratios at the bottom of the trough and allowing them to diffuse towards and adsorb at the interface (schematic overview in Fig. 5). Langmuir-Blodgett (**LB**) films were produced, and the topography of the dried films was analysed using atomic force microscopy (**AFM**) (Fig. 5). There is a narrow concentration range of RPC and OS that could be injected into the trough to induce co-adsorption. As a result, a fixed ratio with various protein concentrations could not be studied, but the RPC-to-OS ratio and the total amount of stabilisers were varied.

The topography of pure RPC showed many white structures, which are thicker regions on the film, and were previously identified as protein-dense regions (Yang, Faber, et al., 2020; Yang, Thielen, et al., 2020). The protein regions (or clusters) are either pre-existing aggregates in the protein material, or are possibly formed because of attractive interactions between the proteins that result in protein segregation (Yang, Thielen, et al., 2020). Jamming of protein-dense regions is responsible for the strain hardening in compression in the Lissajous plots (Fig. 4). The addition of OS in a 100:1 RPC-to-OS ratio resulted in a film with larger protein-dense regions. By carefully examining the film, long strand-like structures can be observed (see arrow in Fig. 5). The strand-like structures were previously identified as membrane fragments of disrupted oleosomes (Yang, Waardenburg, et al., 2021). Similar

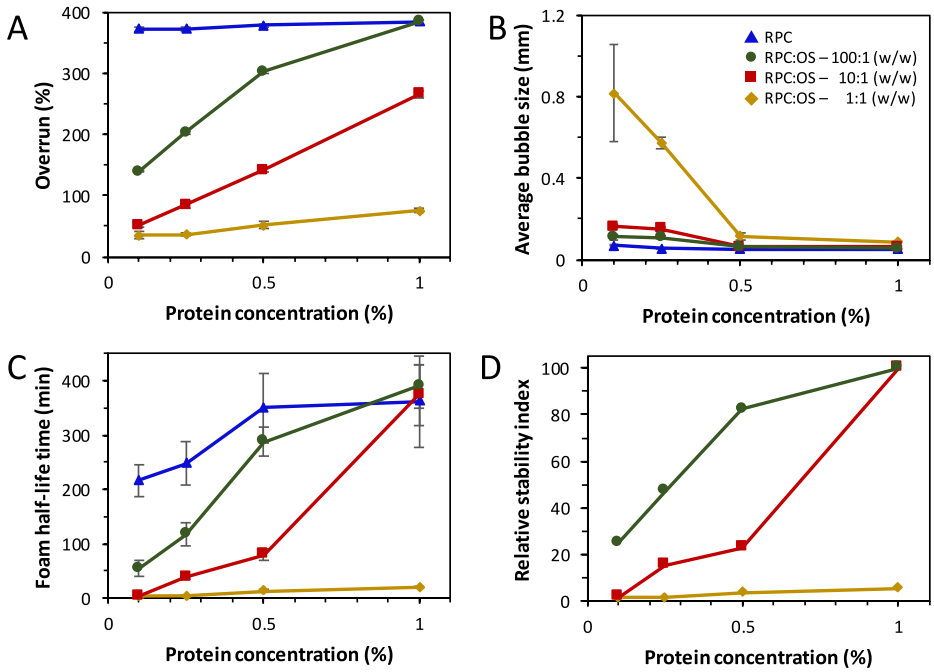


**Fig. 7.** The overrun (A), average bubble size (B, diameter), volume half-life time (C), and relative stability index of foams stabilised by RPC and RPC-OS mixtures. The line drawn through points is to guide the eye. Averages and standard deviations are the result of at least three replicates.

structures were observed earlier on RPC-stabilised films that were made from unfiltered RPC (Yang, Faber, et al., 2020). In the current work, the RPC was filtered over 0.22 μm to remove OS, which resulted in fewer strand-like structures.

Increasing the OS content to a 10:1 RPC-to-OS ratio showed a different topography, as larger structures and flat areas can be observed. The large structures could be intact oleosomes or large protein-dense regions. The flat areas are likely TAG- or phospholipid-rich regions, as demonstrated for pure OS and whey protein-OS mixed interfaces (Waschatko, Schiedt, et al., 2012; Yang, Waardenburg, et al., 2021). A similar topography can be observed by further increasing the OS concentration to a 1:1 RPC-to-OS ratio, as flat regions are still present at the surface. A minor difference between the current work and the one performed on whey protein-OS mixtures is the larger structures at the surface, which could be the formation of large domains of RPC proteins or (intact) OS structures. The presence of intact OS is a noticeable finding, as OS are known to rupture at an air-water interface (Waschatko, Schiedt, et al., 2012). On the other hand, the rupture of sunflower OS at oil-water interfaces was previously found for larger sunflower OS (>1 μm) (Karefyllakis et al., 2019). The smaller sunflower OS (<1 μm) remained intact in the oil-water systems, and the rapeseed OS on our LB films (Fig. 5) were in a small size range (<0.25 μm). This could imply that the large OS ruptured, leading to the formation of the flat lipid-rich regions, whereas the smaller ones remained intact at the interface. At lower RPC-to-OS ratios (i.e. higher OS content), more OS are present in the bulk, which would explain the presence of more intact OS on the LB films.

In conclusion, the co-adsorption of rapeseed proteins and OS resulted in the formation of mixed interfaces, where the OS formed lipid-dense regions between rapeseed proteins. Such 2D-phase separation would lead to weaker in-plane interactions among adsorbed proteins. This was also observed in the dilatational surface rheology, especially for the mixtures at lower protein concentrations (0.1% RPC – 0.01% OS & 0.2% RPC – 0.02% w/w OS) (Fig. 4).

### 3.2.5. *Adsorption behaviour of oleosomes on rapeseed protein interfaces*

In this section, we focus on the interfacial behaviour for RPC-OS mixtures at higher protein concentrations (0.5% RPC – 0.05% OS & 1.0% RPC – 0.1% w/w OS). In the adsorption behaviour (Fig. 2) of these samples, the RPC seemed to dominate the initial adsorption phase. Also, in the surface dilatational rheology (Fig. 4), the rapeseed proteins dictated the mechanical properties of the RPC-OS mixtures. From these results, we hypothesised that OS might not be able to adsorb after the formation of a rapeseed protein-stabilised interfacial film. This hypothesis was investigated by creating LB films in a sequential manner, and a schematic overview of the process is shown in Fig. 6A.

First, a surface pressure isotherm of rapeseed proteins was produced by spreading the RPC solution at the surface of the subphase in the Langmuir trough (Fig. 6B). The isotherm showed an increase in surface pressure upon compression. Here, we observe the formation of an increasingly condensed layer upon compression. Five different compression states, with surface pressures varying from 5 – 25 mN/m, were chosen. After the production of the layers, an OS suspension was infused in the subphase, below the RPC-stabilised Langmuir film. The OS were allowed to diffuse and potentially adsorb at the interface, and, afterwards, Langmuir-Blodgett films were created.

AFM images of the films stabilised with pure RPC, and with RPC and infused OS are shown in Fig. 6C. The pure RPC-stabilised films show the previously mentioned white structures, which are segregated protein-dense regions. When increasing the surface pressure from 5 to 25 mN/m, thus increasing the protein surface concentration, more protein-dense regions can be observed. At the highest compression states corresponding to 20 and 25 mN/m, we observed the formation of highly dense and heterogeneous structures, which was previously also highlighted for whey protein and rapeseed protein-stabilised interfaces (Yang, Faber, et al., 2020; Yang, Thielen, et al., 2020). The formation of such a dense and heterogeneous microstructure was the result of strong in-plane interactions between proteins, which led to the formation of a heterogeneous viscoelastic solid-like interfacial film.

The introduction of OS in the subphase resulted in a different microstructure for the LB films (Fig. 6C) and a shift of the surface pressure. For the 5, 10 and 15 mN/m RPC-stabilised interfaces, the surface pressure increased to 13.6, 13.3, and 15.7 mN/m, respectively (Fig. 6B). The RPC-stabilised interfacial films at 20 and 25 mN/m remained constant upon the introduction of OS. From these surface pressure increases, we can assume that adsorption of OS occurred when

the rapeseed protein-related surface pressure reaches only 5, 10 or 15 mN/m. The presence of intact OS is also clearly visible on the RPC-OS films at 5 and 10 mN/m, as larger structures (100–300 nm) can be observed. Also, more long strand-like structures were present, which were previously identified as membrane fragments upon disruption of the larger OS (Yang, Waardenburg, et al., 2021). At 15 mN/m, no clear visible alterations were present after the introduction of OS. A minor amount of OS could have adsorbed, as the surface pressure increased from 15.0 to 15.7 mN/m, but this was not detected in the topography of the LB films. Further increasing the compression state of the RPC-stabilised interface to 20 or 25 mN/m resulted in RPC-OS films that were comparable with the pure RPC films. This observation, combined with the constant surface pressure after introducing OS, indicates that OS could not adsorb at the interface. Also, OS did not seem to attach as a sublayer beneath the rapeseed protein-stabilised interface, as the formation of such layers would normally result in clear alterations of the film topography, and thus be visible in AFM images.

The OS could not adsorb at the air-water interface when rapeseed proteins formed a condensed interfacial layer. Conversely, they did adsorb at a pre-formed RPC-stabilised interface at lower compression states (≤15 mN/m). We could argue that a loosely covered interface results in weaker in-plane interactions at these lower surface pressures, thus allowing OS to adsorb and probably rupture and spread at the interface. These findings imply that rapeseed proteins can outcompete OS for the air-water interface and avoid the OS from adsorbing, if the proteins can form a dense solid-like interfacial layer. This proposed mechanism is also reflected in the mechanical properties (Fig. 4) of RPC-OS mixture-stabilised interfaces (0.5% RPC – 0.05% OS & 1.0% RPC – 0.1% w/w OS), where the rapeseed proteins dictated the rheological behaviour. Another interesting point is the entrapment of phospholipids in the colloidal structure of the OS. Phospholipids can be detrimental for a protein-stabilised interface, and may displace proteins from the interface (Denkov & Marinova, 2006; Pichot, Watson, & Norton, 2013). In the present case, the lipid molecules in the OS did not have such an effect, probably because they are trapped in the OS structure.

### 3.3. Foaming properties of rapeseed protein – oleosome mixtures

The foaming properties of three RPC-to-OS ratios (100:1, 10:1, 1:1) were studied at fixed protein concentrations between 0.1 – 1.0% (w/w) (Fig. 7). A wide range of RPC-to-OS ratios was studied to evaluate the effect of OS on RPC-stabilised foams at various OS concentrations. First, the foaming ability was studied by measuring the overrun and average air bubble size. The overrun was expressed as the foam volume over the initial liquid volume. RPC-stabilised foams had high overruns between 372 – 384% (Fig. 7A). Increasing the OS concentration to a 100:1 RPC-to-OS ratio resulted in lower overruns for foams with protein concentrations ranging from 0.1 – 0.5% (w/w) compared to pure RPC, whereas the RPC-OS mixture with 1.0% (w/w) protein had a similar overrun as a pure 1.0% (w/w) RPC foam. The detrimental effect of OS was higher at lower protein concentrations. Such a trend was also present by further increasing the OS concentration to a 10:1 and 1:1 RPC-to-OS ratio, as the overrun increased at higher protein content at the same RPC-to-OS ratio. The addition of OS (from 100:1 to 1:1 ratio) initiated a decrease in foam overrun at each concentration, but the detrimental effect was less marked at higher protein concentrations.

A similar trend was also observed in the average air bubble size (Fig. 7B), as the bubble size became larger when increasing OS concentration (100:1 to 1:1 ratio). At 0.1% (w/w), the largest increase of air bubble size could be observed, which increased from 0.07 (pure RPC) to 0.82 mm (1:1 ratio), whereas increasing the protein concentration to 1.0% (w/w) resulted in an increase from 0.05 mm to 0.09 mm. Also, the OS hampered the air bubble formation more at lower protein concentrations. From the interfacial rheology experiments, it was obvious that OS reduced the in-plane interactions among adsorbed proteins, which are required for proteins to form stiff and solid-like layers around air bubbles. As a result, the formed interfaces were weaker, leading to a collapse of air bubbles already during the foam formation, thus resulting in larger air bubbles at the moment of recording. We also attempted to create foams using pure OS solutions with bulk concentrations ranging from 0.01 – 1.0% (w/w), but no foams could be created. The absence of foamability by OS is most likely attributed to the formation of a weak and incohesive interfacial layer due to the rupture and spreading of free TAGs and phospholipids. The presence of free lipids was previously found to be detrimental to the protein connectivity at the interface, thus substantially reducing the foaming properties of proteins (Denkov, 2004; Wilde et al., 2003; Yang, Waardenburg, et al., 2021).

The presence of OS also affected the foam stability, which was evaluated by determining the time point where half of the foam volume decays, also known as the foam volume half-life time (Fig. 7C). RPC-stabilised foams had half-life times increasing from 216 min at 0.1% (w/w) to 362 min at 1.0% (w/w) protein bulk concentration, and the addition of OS to RPC resulted in a decrease in foam half-life times. To directly compare the influence of OS on RPC-stabilised foams, a relative stability index was calculated by dividing the half-life time of an RPC–OS–stabilised foam over the half-life time of a pure RPC-stabilised foam at the same protein concentration times 100 (Fig. 7D). At the lowest protein concentration of 0.1% (w/w), the relative stability index decreased to 25.2 at a 100:1 ratio and even further to 1.6 at a 1:1 ratio. The foam stabilised with 1.0% (w/w) protein had a relative stability index of 100 at 100:1 and 10:1 ratio, suggesting no negative influence of OS. The influence of OS on foam stability of RPC was more detrimental at lower protein concentrations at each ratio, and by increasing OS concentration (100:1 to 1:1 ratio).

The interfacial rheology experiments showed the formation of weaker protein layers with reduced connectivity due to the presence of free TAGs and phospholipids after OS rupture, thus decreasing foaming ability and stability. Lipid droplets are also known to play a destabilising effect in the thin films between the interfacial layers of two neighbouring air bubbles. One of the proposed anti-foaming mechanisms is bridging by the droplet in the thin film, where the droplet connects air-water interfaces between two air bubbles. Afterwards, the surface material around to droplet can spread and replace the proteins on the film. At this point, the thin film is connected by an unstable oil bridge, which can cause film rupture (Denkov, 2004; Denkov & Marinova, 2006). OS seem to behave as anti-foaming agents in the early stages of foam preparation, as OS can influence the air bubble size and foam overrun. The formation of larger air bubbles is correlated to lower foam stability, as the entrapped liquid in the foam is lower and gas diffusion through the films is higher compared to foams with smaller air bubbles.

The anti-foaming effect of OS is the highest at low protein concentrations (0.1 and 0.2%), where the protein film is probably less dense due to lower protein concentrations. The OS can likely perform film bridging in these conditions and also adsorb at the interface, followed by spreading and film rupture, as shown by rheology (Fig. 4) and microstructure imaging (Fig. 6). These techniques also showed the formation of an RPC-dominated interface at higher protein concentrations. As a result, the negative effect of OS on foam/air bubble formation and stability decreased. Additionally, we could argue that OS might be trapped between the air bubbles, as observed for hydrophilic particles (Aveyard, Beake, & Clint, 1996). The entrapment of the hydrophilic OS in lamellae and plateau borders could prevent the rupture at the interface, thus protecting the protein-stabilised interface and foam from destabilising. However, the 'protective' effect of a stiff and dense protein layer reduced at higher OS concentrations, leading to more extensive film-bridging, even at a high fixed RPC concentration of 1.0% (w/w). At these concentrations, the rapeseed proteins might not be able to outcompete the higher number of OS for the interface, or more extensive film-bridging could occur.

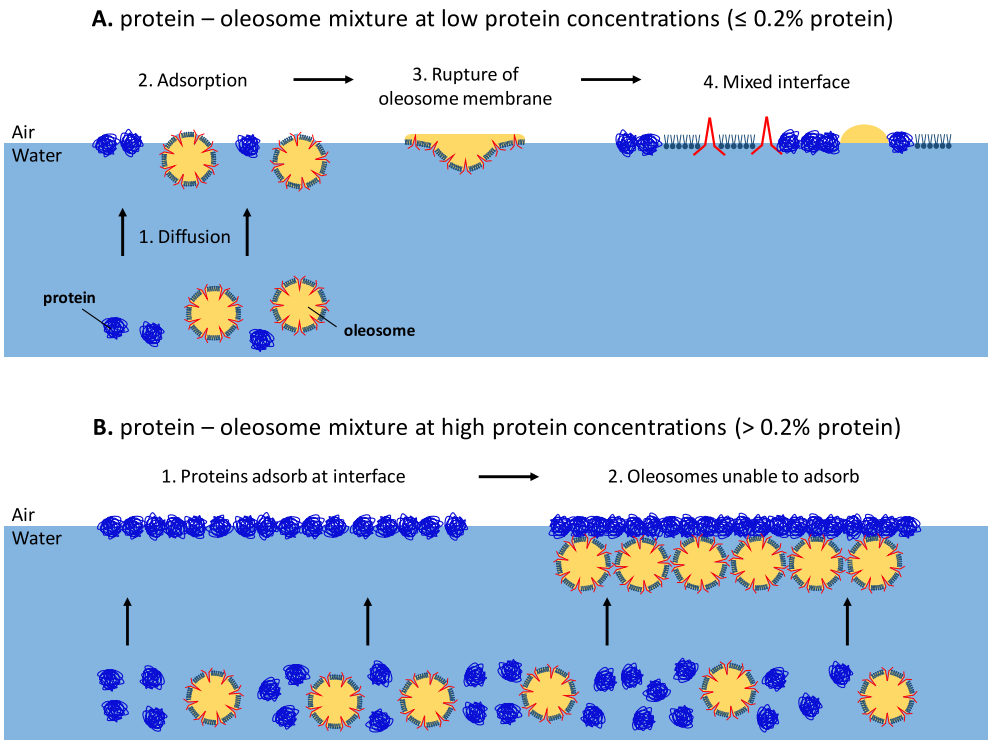


**Fig. 8.** A schematic representation of the proposed interface stabilisation mechanism of rapeseed protein concentrate (RPC) – oleosome (OS) mixtures.

## 4. Conclusion

In this work, the influence of oleosomes (OS) on rapeseed protein concentrate (RPC)-stabilised interfacial films and foams were investigated. At low protein concentrations (0.1 and 0.2% w/w), RPC and OS co-adsorb at the interface, resulting in a weaker interfacial layer than that formed with pure RPC. The OS can unfold at the interface, and their lipid components (phospholipids and TAGs) can spread and decrease the connectivity between the adsorbed proteins (Fig. 8A). As a result, in the presence of OS in these conditions, the foaming ability and stability of RPC decrease. The OS are probably able to adsorb and rupture due to a loosely packed protein interface.

At higher protein concentrations (0.5 and 1.0% w/w), rapeseed proteins dominate the interfacial properties, and OS have a less detrimental effect on the foaming properties compared to the situation at a low protein concentration. By infusing an OS suspension beneath a preformed RPC-stabilised Langmuir film (Fig. 8B), we demonstrated that OS are not able to adsorb at such an interface when the rapeseed proteins have readily formed a dense layer with a surface pressure of >15 mN/m. At high enough concentrations, the rapeseed proteins thus outcompete the OS interfacial localisation. This interface stabilisation mechanism could protect the protein foams from the detrimental effect of OS. However, at a high OS concentration and lower ratios (RPC:OS ratio of 1:1), OS act as effective anti-foaming agents, since the foam stability was reduced by more than 98% compared to the pure RPC-stabilised systems. We should also keep in mind that rapeseed protein concentrate is a mixture of two types of proteins (i.e. napin and cruciferin). It would be of great interest for future studies to evaluate the exact role of each protein in the competition with OS for the interface.

In summary, we have demonstrated that the influence of OS on RPC interfacial and foaming properties can be tuned by changing the RPC-to-OS ratio or the absolute amount of stabiliser up to a certain degree. The relationship between foaming properties and the concentration of bulk material is promising for the application of OS in aerated food systems. OS could be co-extracted with plant proteins or separately introduced as a sustainable ingredient and lipid source. The utilisation of oleosomes should be further explored in both academia and the food industry, as oleosomes can play an important role in producing healthy and sustainable food products.

## Declaration of competing interest

The authors have declared that no competing interest exist. This manuscript has not been published and is not under consideration for publication in any other journal. All authors approve this manuscript and its submission to Food Hydrocolloids.

## Acknowledgements

The authors thank Helene Mocking for her contribution to the extraction of the rapeseed protein concentrate. The authors have declared that no competing interest exists. The project is funded by TiFN, a public-private partnership on precompetitive research in food and nutrition. The public partners are responsible for the study design, data collection and analysis, decision to publish, and preparation of the manuscript. The private partners have contributed to the project through regular discussion. This research was performed with additional funding from the Netherlands Organisation for Scientific Research (NWO), and the Top Consortia for Knowledge and Innovation of the Dutch Ministry of Economic Affairs (TKI). NWO project number: ALWTF.2016.001.

## References

Abdullah, Weiss, J., & Zhang, H. (2020). Recent advances in the composition, extraction and food applications of plant-derived oleosomes. *Trends in Food Science & Technology, 106*(September), 322–332. https://doi.org/10.1016/j.tifs.2020.10.029

Aveyard, R., Beake, B. D., & Clint, J. H. (1996). Wettability of spherical particles at liquid surfaces. *Journal of the Chemical Society, Faraday Transactions, 92*(21), 4271–4277. https://doi.org/10.1039/ft9969204271

Caro, A. L., Niño, M. R. R., & Patino, J. M. R. (2009). The effect of pH on structural, topographical, and rheological characteristics of β-casein-DPPC mixed monolayers spread at the air-water interface. *Colloids and Surfaces A: Physicochemical and Engineering Aspects, 332*(2–3), 180–191. https://doi.org/10.1016/j.colsurfa.2008.09.020

Damodaran, S. (2005). Protein stabilization of emulsions and foams. *Journal of Food Science, 70*(3), R54–R66. https://doi.org/10.1111/j.1365-2621.2005.tb07150.x

Damude, H. G., & Kinney, A. J. (2008). Enhancing plant seed oils for human nutrition. *Plant Physiology, 147*(3), 962–968. https://doi.org/10.1104/pp.108.121681

Danlami, J. M., Arsad, A., Zaini, M. A. A., & Sulaiman, H. (2014). A comparative study of various oil extraction techniques from plants. *Reviews in Chemical Engineering, 30*(6), 605–626. https://doi.org/10.1515/revce-2013-0038

Denkov, N. D. (2004). Mechanisms of foam destruction by oil-based antifoams. *Langmuir, 20*(22), 9463–9505. https://doi.org/10.1021/la049676o

Denkov, N. D., & Marinova, K. G. (2006). Antifoam effects of solid particles, oil drops and oil–solid compounds in aqueous foams. In *Colloidal particles at liquid interfaces* (pp. 383–444). https://doi.org/10.1017/CBO9780511536670.011

Dickinson, E. (1999). Adsorbed protein layers at fluid interfaces: Interactions, structure and surface rheology. *Colloids and Surfaces B: Biointerfaces, 15*(2), 161–176. https://doi.org/10.1016/S0927-7765(99)00042-9

Dickinson, E. (2011). Mixed biopolymers at interfaces: Competitive adsorption and multilayer structures. *Food Hydrocolloids, 25*(8), 1966–1983. https://doi.org/10.1016/j.foodhyd.2010.12.001

Ding, J., Wen, J., Wang, J., Tian, R., Yu, L., Jiang, L., et al. (2020a). The physicochemical properties and gastrointestinal fate of oleosomes from non-heated and heated soymilk. *Food Hydrocolloids, 100*(October 2019), 105418. https://doi.org/10.1016/j.foodhyd.2019.105418

Ding, J., Xu, Z., Qi, B., Liu, Z., Yu, L., Yan, Z., et al. (2020b). Thermally treated soya bean oleosomes: The changes in their stability and associated proteins. *International Journal of Food Science and Technology, 55*(1), 229–238. https://doi.org/10.1111/ijfs.14266

Ewoldt, R. H., Hosoi, A. E., & McKinley, G. H. (2007). New measures for characterizing nonlinear viscoelasticity in large amplitude oscillatory shear. *Journal of Rheology, 52*(6), 1427–1458. https://doi.org/10.1122/1.2970095

Fetzer, A., Herfellner, T., & Eisner, P. (2019). Rapeseed protein concentrates for non-food applications prepared from pre-pressed and cold-pressed press cake via acidic precipitation and ultrafiltration. *Industrial Crops and Products, 132*, 396–406. https://doi.org/10.1016/j.indcrop.2019.02.039

Foegeding, E. A., Luck, P. J., & Davis, J. P. (2006). Factors determining the physical properties of protein foams. *Food Hydrocolloids, 20*(2–3), 284–292. https://doi.org/10.1016/j.foodhyd.2005.03.014

Frandsen, G. I., Mundy, J., & Tzen, J. T. C. (2001). Oil bodies and their associated proteins, oleosin and caleosin. *Physiologia Plantarum, 112*(3), 301–307. https://doi.org/10.1034/j.1399-3054.2001.1120301.x

Glomm, W. R., Volden, S., Halskau, Ø., & Ese, M. H. G. (2009). Same system-different results: The importance of protein-introduction protocols in Langmuir-monolayer studies of lipid-protein interactions. *Analytical Chemistry, 81*(8), 3042–3050. https://doi.org/10.1021/ac8027257

Humblet-Hua, N.-P. K., van der Linden, E., & Sagis, L. M. C. (2013). Surface rheological properties of liquid–liquid interfaces stabilized by protein fibrillar aggregates and protein–polysaccharide complexes. *Soft Matter, 9*(7), 2154–2165. https://doi.org/10.1039/c2sm26627j

Ishii, T., Matsumiya, K., Nambu, Y., Samoto, M., Yanagisawa, M., & Matsumura, Y. (2017). Interfacial and emulsifying properties of crude and purified soybean oil bodies. *Food Structure, 12*, 64–72. https://doi.org/10.1016/j.foostr.2016.12.005

Iwanaga, D., Gray, D. A., Fisk, I. D., Decker, E. A., Weiss, J., & McClements, D. J. (2007). Extraction and characterization of oil bodies from soy beans: A natural source of pre-emulsified soybean oil. *Journal of Agricultural and Food Chemistry, 55*(21), 8711–8716. https://doi.org/10.1021/jf071008w

Kapchie, V. N., Yao, L., Hauck, C. C., Wang, T., & Murphy, P. A. (2013). Oxidative stability of soybean oil in oleosomes as affected by pH and iron. *Food Chemistry, 141*(3), 2286–2293. https://doi.org/10.1016/j.foodchem.2013.05.018

Karefyllakis, D., Van Der Goot, A. J., & Nikiforidis, C. V. (2019). The behaviour of sunflower oleosomes at the interfaces. *Soft Matter, 15*(23), 4639–4646. https://doi.org/10.1039/c9sm00352e

Karkani, O. A., Nenadis, N., Nikiforidis, C. V., & Kiosseoglou, V. (2013). Effect of recovery methods on the oxidative and physical stability of oil body emulsions. *Food Chemistry, 139*(1–4), 640–648. https://doi.org/10.1016/j.foodchem.2012.12.055

Lin, L., Allemekinders, H., Dansby, A., Campbell, L., Durance-Tod, S., Berger, A., et al. (2013). Evidence of health benefits of canola oil. *Nutrition Reviews, 71*(6), 370–385. https://doi.org/10.1111/nure.12033

Mackie, A. R., Gunning, A. P., Wilde, P. J., & Morris, V. J. (1999). Orogenic displacement of protein from the air/water interface by competitive adsorption. *Journal of Colloid and Interface Science, 210*(1), 157–166. https://doi.org/10.1006/jcis.1998.5941

Maldonado-Valderrama, J., & Patino, J. M. R. (2010). Interfacial rheology of protein-surfactant mixtures. *Current Opinion in Colloid & Interface Science, 15*(4), 271–282. https://doi.org/10.1016/j.cocis.2009.12.004

Narsimhan, G., & Xiang, N. (2018). Role of proteins on formation, drainage, and stability of liquid food foams. *Annual Review of Food Science and Technology, 9*, 45–63. https://doi.org/10.1146/annurev-food-030216-030009

Nikiforidis, C. V. (2019). Structure and functions of oleosomes (oil bodies). *Advances in Colloid and Interface Science, 274*, 102039. https://doi.org/10.1016/j.cis.2019.102039

Ntone, E., Bitter, J. H., & Nikiforidis, C. V. (2020). Not sequentially but simultaneously: Facile extraction of proteins and oleosomes from oilseeds. *Food Hydrocolloids, 102*, 105598. https://doi.org/10.1016/j.foodhyd.2019.105598

Pichot, R., Watson, R. L., & Norton, I. T. (2013). Phospholipids at the interface: Current trends and challenges. *International Journal of Molecular Sciences, 14*(6), 11767–11794. https://doi.org/10.3390/ijms140611767

Romero-Guzmán, M. J., Köllmann, N., Zhang, L., Boom, R. M., & Nikiforidis, C. V. (2020). Controlled oleosome extraction to produce a plant-based mayonnaise-like emulsion using solely rapeseed seeds. *Lebensmittel-Wissenschaft & Technologie, 123*, 109120. https://doi.org/10.1016/j.lwt.2020.109120

Romero-guzman, M. J., Louis, L. J., Kyriakopoulou, K., Boom, R. M., & Nikiforidis, C. V. (2020). Efficient Single-Step Rapeseed Oleosome Extraction Using Twin-Screw Press. *J. Food Eng., 276*, 109890. https://doi.org/10.1016/j.jfoodeng.2019.109890.

Tasan, M., Gecgel, U., & Demirci, M. (2011). Effects of storage and industrial oilseed extraction methods on the quality and stability characteristics of crude sunflower oil (Helianthus annuus L.). *Grasas Y Aceites, 62*(4), 389–398. https://doi.org/10.3989/gya.126010

Tzen, J. T. C. (2012). Integral proteins in plant oil bodies. *ISRN Botany*, 1–16. https://doi.org/10.5402/2012/173954, 2012.

Tzen, J. T. C., Cao, Y. Z., Laurent, P., Ratnayake, C., & Huang, A. H. C. (1993). Lipids, proteins, and structure of seed oil bodies from diverse species. *Plant Physiology, 101*(1), 267–276. https://doi.org/10.1104/pp.101.1.267

Waninge, R., Walstra, P., Bastiaans, J., Nieuwenhuijse, H., Nylander, T., Paulsson, M., et al. (2005). Competitive adsorption between β-casein or β-lactoglobulin and model milk membrane lipids at oil-water interface. *Journal of Agricultural and Food Chemistry, 53*(3), 716–724. https://doi.org/10.1021/jf049267y

Waschatko, G., Junghans, A., & Vilgis, T. A. (2012a). Soy milk oleosome behaviour at the air-water interface. *Faraday Discussions, 158*, 157–169. https://doi.org/10.1039/c2fd20036h

Waschatko, G., Schiedt, B., Vilgis, T. A., & Junghans, A. (2012b). Soybean oleosomes behavior at the air − water interface. *The Journal of Physical Chemistry B, 116*, 10832–10841. https://doi.org/10.1021/jp211871v

Wilde, P. J., Wilde, P. J., Husband, F. a, Husband, F. a, Cooper, D., Cooper, D., et al. (2003). Destabilization of beer foam by lipids: Structural and interfacial effects. *Journal of the American Society of Brewing Chemists, 61*, 196–202. https://doi.org/10.1094/ASBCJ-61-0196

Yang, J., Faber, I., Berton-Carabin, C. C., Nikiforidis, C. V., van der Linden, E., & Sagis, L. M. C. (2020a). Foams and air-water interfaces stabilised by mildly purified rapeseed proteins after defatting. *Food Hydrocolloids, 112*, 106270. https://doi.org/10.1016/j.foodhyd.2020.106270

Yang, J., Lamochi Roozalipour, S. P., Berton-Carabin, C. C., Nikiforidis, C. V., van der Linden, E., & Sagis, L. M. C. (2021a). Air-water interfacial and foaming properties of whey protein - sinapic acid mixtures. *Food Hydrocolloids, 112*, 106467. https://doi.org/10.1016/j.foodhyd.2020.106467

Yang, J., Thielen, I., Berton-Carabin, C. C., van der Linden, E., & Sagis, L. M. C. (2020b). Nonlinear interfacial rheology and atomic force microscopy of air-water interfaces stabilized by whey protein beads and their constituents. *Food Hydrocolloids, 101*, 105466. https://doi.org/10.1016/j.foodhyd.2019.105466

Yang, J., Waardenburg, L. C., Berton-Carabin, C. C., Nikiforidis, C. V., van der Linden, E., & Sagis, L. M. C. (2021b). Air-water interfacial behaviour of whey protein and rapeseed oleosome mixtures. *Journal of Colloid and Interface Science, 602*, 207–221. https://doi.org/10.1016/j.jcis.2021.05.172

Zhang, H., Cui, G., & Li, J. (2002). Morphological investigation of mixed protein/phospholipid monolayers. *Colloids and Surfaces A: Physicochemical and Engineering Aspects, 201*(1–3), 123–129. https://doi.org/10.1016/S0927-7757(01)00879-2